Soft Matter

Accepted Manuscript

ROYAL SOCIETY OF CHEMISTRY

www.rsc.org/softmatter

Soft Matter

PAPER

Revealing the Dynamic Heterogeneity of PMMA/PVDF Blends: From the Microscopic Dynamics to Macroscopic Properties

Received 00th January 20xx,
Accepted 00th January 20xx

DOI: 10.1039/x0xx00000x

www.rsc.org/

Bo Lu,[a] Khalid Lamnawar,[b*] Abderrahim Maazouz[ac*] and Huagui Zhang[ad]

An effort was made to demonstrate the dynamic heterogeneity of poly(methyl methacrylate) (PMMA)/poly(vinylidene fluoride) (PVDF) blends, where its composition dependence and the role of interphase were probed. Firstly, the composition dependence of thermorheological complexity of PMMA/PVDF blends in the melt was revealed. Molecular entanglement state involving intra- and interchain entanglements was found to govern the scenario of thermorheological complexity. Intriguingly, local heterogeneity was further demonstrated to exist in the melt-state blends with intermediate compositions, and its origin was depicted to be the interphase. The interphase, coupled with unfavourable interchain entanglements in those blends, could explain the reduced viscosity and speed-up relaxations, contributing to the overall thermorheological complexity. Besides, two experimental glass transition temperatures of blends were resolved in view of segment motions in the miscible phase and the crystal-amorphous interphase, and further assessed via the "self-concentration" concept. The presence of a crystal-amorphous interphase, likely leading to three distinct dynamics of segments in blends, was supposed to contribute to the dynamic heterogeneity in segment relaxations for PMMA/PVDF blends at the solid state. Lastly, effects of dynamic heterogeneity on dynamic mechanical properties were also evaluated.

1 Introduction

With increasing demand for suitable polymer electrolytes in advanced electrochemical applications (*e.g.* lithium-ion battery) nowadays, polymer blends once again aroused public attentions and have been increasingly considered as the most promising and feasible approach. Among them, blends of PMMA/PVDF have attracted the sustained interest due to their tunable mechanical and electrochemical properties, ease of fabrication and good contact with electrode materials, etc.[1-3] Design of tailor-made electrolytes based on PMMA/PVDF blends would be enormously facilitated by the understanding of the blending phenomenon at a molecular level. It is generally stated that blends of PMMA and PVDF are completely miscible in the melt state at all compositions, due to the strong intermolecular interactions involving hydrogen bonding between carbonyl groups in PMMA and -CH_2 groups of PVDF, and the dipole−dipole interactions between -CH_2 of PMMA and -CF_2 in PVDF. A single calorimetric glass transition temperature (T_g) is usually taken as the proof for the miscibility of PMMA/PVDF blends.[4-6] Whereas, the width of the glass transition of this pair of blends is always broader than those of components.[7, 8] The broadness of glass transition has been also observed in many miscible blends and generally attributed to the heterogeneity in structural relaxations, *i.e.* dynamic heterogeneity. Dynamic heterogeneity has been intensively studied in the past two decades particularly with several typical miscible blends as models: polyisoprene (PI)/poly(vinylethylene) (PVE),[9-12] PI/polybutadiene (PB),[13-15] PMMA/ poly(ethylene oxide) (PEO),[16-18] etc. Relevant studies addressing this topic have been comprehensively elaborated in recent review articles.[19-21] Concentration fluctuations[22, 23] and chain connectivity effects are generally considered to be responsible for the dynamic heterogeneity. [24, 25] Specifically, the latter emphasizes the self-concentration, value of which is approximately ratio of the packing volume of a Kuhn length's worth of monomers to the cooperative volume.[24]

With a substantial dynamic asymmetry (ΔT_g=150K), PMMA/PVDF blends are also supposed to be dynamically heterogeneous. In a pioneering work, Han and co-workers[26] demonstrated that the temperature dependence of time-temperature shift factor for PMMA/PVDF varies with blend composition and predicted the failure of empirical Time-Temperature Superposition (TTS) principle. Though Yousefi and co-workers[27] later observed the breakdown of TTS principle in PMMA/PVDF blend and claimed its thermorheological complexity, the blends under their study were within a narrow range of compositions. A clear conclusion has not yet been drawn as strong intermolecular interactions in

[a] Université de Lyon, CNRS, UMR 5223, Ingénierie des Matériaux Polymères, INSA Lyon, F-69621, Villeurbanne, France.
E-mail: abderrahim.maazouz@insa-lyon.fr
[b] Université de Lyon, CNRS, UMR 5259, LaMCoS, Laboratoire de Mécanique des Contacts et des Structures, INSA Lyon, F-69621, Villeurbanne, France.
E-mail: khalid.lamnawar@insa-lyon.fr
[c] Hassan II Academy of Science and Technology, Rabat, Morocco
[d] School of Chemical and Process Engineering, University of Leeds, LS2 9JT, Leeds, UK

† Electronic Supplementary Information (ESI) available: FTIR spectra of blends and analyses, dielectric data (loss permittivity, Cole-cole plots, conductivity) and discussions, DSC results. See DOI: 10.1039/x0xx00000x

PMMA/PVDF blends that could affect their thermorheological complexity/simplicity. While a detailed investigation is needed to understand the thermorheological complexity for PMMA/PVDF blends, it is well understood that their interactions are strongly composition-dependent.[4, 6] In most miscible blends, the intermolecular interactions influence remarkably the thermorheological complexity.[28, 29] The degree of thermorheological complexity for PMMA/PVDF blends might also vary with composition, which, however, has until now been largely ignored in the literature. Besides, chain entanglements strongly influence the intermolecular coupling and cooperativity between chains, thus determining the thermorheological complexity or simplicity.[7] Though chain entanglements of PMMA/PVDF blends were studied by several researchers, apparently conflicting results have been obtained. Wu[30] found that dissimilar chains are less likely to entangle with each other than the similar chains in PMMA/PVDF blends over the wide range of compositions. In a recent study, however, Zuo and co-workers[31] reported a completely opposite result that dissimilar chains are more likely to entangle with each other than the similar chains for the PMMA/PVDF blends. Obviously, a clear consensus has not yet been reached regarding the chain entanglement and its relationship with thermorheological complexity of PMMA/PVDF blends.

Furthermore, upon cooling from the melt, PMMA/PVDF blends show upper critical solution temperature (UCST) strongly dependent on the blend composition and the cooling rate. They undergo liquid-liquid and crystallization-induced phase separation in sequence. PVDF in the blends can either crystallize or remain amorphous depending on blend composition and the cooling rate.[32] No crystallization takes place in blends with PVDF content below 40 wt% either upon slow cooling from the melt or by annealing at the temperature above T_g, leading to the morphology as a single amorphous phase. In contrast, blends with PVDF concentration above 40 wt% can crystallize from the melt and phase separation occurs subsequently. The resulting multiphase morphology of crystalline blends consists of a crystalline PVDF phase, an amorphous miscible PMMA/PVDF phase, together with a crystalline-amorphous interphase.[32, 33] Particularly, the liquid-like interphase is solely comprised of amorphous PVDF segments.[32, 34] Both the rigid PMMA segments in the miscible phase and the PVDF crystals impose confinement on the dynamics of the amorphous PVDF segments, and the relaxation dynamics of the interphase therefore vary as a function of composition.[32] Besides, two experimental T_gs related to the multiphase morphology were even reported for crystalline PMMA/PVDF blends,[7, 30] suggesting the structural heterogeneities in these blends. However, the corresponding molecular origins and relevant segmental dynamic heterogeneity are still unsolved in the open literatures. Furthermore, it is noteworthy that PVDF chains possess the strong tendency to be self-associated rather than entangled with PMMA chains.[27, 30] This can be probably evidenced by the crystalline-amorphous interphase which is pure PVDF rather than penetrated by PMMA, despite their favourable interactions.[32] Understandably, upon melting the multiphase crystalline blends, the regions containing original PVDF crystal and interphase, *i.e.* PMMA-free regions, will be penetrated and subsequently entangled with PMMA chains. In view of the self-association character of PVDF chains and the unfavourable interchain entanglements between PMMA and PVDF chains, one might imagine that the final state of those regions is not exactly the same as that of the remaining ones and behave as interphase, resulting in two distinct environments in the melt. The presence of interphase in the melt might remarkably affect the molecular dynamics and rheological properties of blends. Whereas, few studies are available in the open literature addressing the effects of interphase on the dynamic heterogeneity and thermorheological behaviors in the melt-state PMMA/PVDF blends.

In this paper, we present a comprehensive view of the dynamic heterogeneity of PMMA/PVDF blends. This is mainly accomplished by performing melt rheology and dielectric relaxation spectroscopy for blends over a wide range of composition, at different melt temperatures. One of the primary objectives is to map the thermorheological complexity and chain entanglement state as a function of composition, and subsequently clarify the relation between them. Based on this, we further attempt to understand the presence of interphase in the melt and its effects on the thermorheological behaviours of blends. Further, effects of heterogeneity related to the crystal-amorphous interphase in the solid-state blends on glass transition temperatures and dynamic mechanical properties will be also evaluated. This paper will offer some new enlightenment for the dynamic studies of PMMA/PVDF blends and their advanced applications.

2 Experimental

2.1 Materials and sample preparation

Table 1 Characteristics of the investigated polymers

	M_w [a] (kg/mol)	M_w/M_n [a]	T_g [b] (°C)	T_m [b] (°C)	T_c [b] (°C)	ρ (g/cm^3)
PVDF	210	2.0	-42	170	136	1.78
PMMA	100	1.9	112	-	-	1.19

[a] Determined by size exclusion chromatography (SEC) with tetrahydrofuran (THF) as the eluent for PMMA and dimethyl formamide (DMF) for PVDF. [b] Measured with a DSC (Q20, TA Instruments) at a heating/cooling rate of 10 °C/min under N_2.

PMMA (Altuglas V825) and PVDF (Kynar 720) in granular pellet form were kindly provided by Arkema Inc. More information about the characteristics of these polymers has been described elsewhere in our previous studies.[7] PMMA/PVDF blends with compositions ranging from 100/0 (v/v) to 0/100 (v/v) with a step of 10 were prepared by melt blending at 220 °C using a twin-screw extruder. Details on the processing procedures were given elsewhere.[35] All

the pristine polymers were dried in a vacuum oven at 80 °C for 48 h prior to blend preparation. As-prepared blends were subsequently compression-molded into disks and rectangular sheets at 200 °C with a pressure of 200 bar. All the samples were further dried at 80 °C under vacuum for at least 24 h before measurements.

2.2 Small-amplitude oscillatory shear (SAOS) measurements

Linear viscoelastic properties of the blends were studied using a stress-controlled rotational rheometer (Discovery Hybrid Rheometer, DHR-2, TA Instruments) with a parallel-plate geometry (25 mm in diameter) at temperatures from 180 to 240 °C under a nitrogen atmosphere. Disk-shaped samples with the thickness of *ca.* 1.2 mm were positioned between the plates, and left for 5 min at the measured temperature to minimize any residual stress and also to improve the adhesion between samples and the plates. To ensure that all the SAOS measurements were performed within the linear viscoelastic regime, a dynamic strain sweep test was first conducted in a strain amplitude range from 0.01% to 100% with a maximum angular frequency (ω) amplitude of 628 rad/s. Then dynamic frequency sweep tests were carried out under a fixed strain amplitude of 5%, which fell well within in the linear viscoelastic region, from the angular frequency of 628 to 0.01 rad/s.

2.3 Dielectric relaxation spectroscopy (DRS)

Dielectric relaxation measurements were conducted on a dielectric thermal analyzer (LCR Meter, Agilent E4980A, TA Instruments) equipped with the Environmental Test Chamber (ETC, TA Instruments) for temperature control. Disk-shaped samples were placed between two parallel-plate brass electrodes (25 mm in diameter) in a way similar to SAOS experiments. Dielectric responses were recorded isothermally for frequency range from 20 Hz to 2 MHz under a constant voltage of 2 V at temperatures from 180 to 240 °C on heating with an increment of 5 °C. Prior to tests, it was also necessary to heat the assembly thereby sticking the polymer to the electrodes. Nitrogen purging was also maintained throughout the tests. Temperature fluctuations were well controlled within ± 0.5 °C.

2.4 Fourier transform infrared spectroscopy (FTIR)

Infrared spectra of the blends were collected on a FTIR spectrometer (Spectrum One, Perkin Elmer Instrument) equipped with an attenuated total reflectance (ATR) device. A reflectance mode combined with 40 scans, a spectral range of 4000–600 cm^{-1} and a resolution of 4 cm^{-1} was used. FTIR samples were prepared by squeezing blend granules into films (thickness *ca.* 30μm) at 200 °C by the compressor.

2.5 Differential scanning calorimetry (DSC)

Calorimetric measurements were performed on a differential scanning calorimeter (DSC, Q20, TA Instruments) in a dry nitrogen atmosphere. A temperature program was set in which the samples were first heated from -90 to 220 °C, then cooled to -90 °C followed by a second heating scan to 220 °C. Both the heating and cooling rates were 10 °C/min. The melting temperature (T_m) and glass transition temperature (T_g) were determined from both first and second heating scan. T_m was noted as the maximum of the melting peak and T_g as the inflection point of the glass transition. The crystallization temperature (T_c) was taken from the maximum of exothermal peak in the cooling run.

2.6 Dynamic mechanical analysis (DMA)

Dynamic mechanical properties of the blends were studied on compression-molded rectangular samples (30 mm × 6 mm × 1.2 mm) using a dynamic mechanical analyzer (DMA, Q800, TA Instruments) in the tensile mode. DMA thermograms were recorded at a constant frequency of 1 Hz, strain amplitude of 0.1%, and heating rate of 2 °C/min over the range from -100 to 180 °C under a nitrogen atmosphere. T_g was also determined from the peak temperature in loss modulus of DMA.

3 Results and discussion

3.1 Linear viscoelasticity of PMMA/PVDF blends: themorheological complexity

Complex viscosity (η^*) of the blends is plotted as a function of angular frequency at a given temperature of 220 °C in Fig. 1a. As observed, the neat polymers and their blends display a shear-thinning behaviour at higher frequencies and a Newtonian behaviour at lower frequencies. PVDF exhibits a moderate shear-thinning behaviour and is less viscous than PMMA. η^* of the blends decreases with the inclusion of PVDF, indicating the formulation of the blends. It is worth noting that η^* of the blends with higher PVDF concentrations especially for the intermediate compositions are lower than those of the neat polymers. Specifically, blend with approximate 70% of PVDF shows the lowest viscosity. The reduction of dynamic viscosity is pretty surprising and will be discussed later. TTS principle has been frequently applied to examine if there exists a rheological heterogeneity and thereby thermorheological complexity in blends. Based on the principle that all the relaxation times are affected in the same degree at different temperatures, a master curve at a reference temperature (T_{ref}) can be generated from viscoelastic data, using a time-temperature shift factor. The validity of TTS can be firstly examined by Han plot with storage modulus (G') versus loss modulus (G'').[36, 37] Fig. 1b presents the Han plots for the blends varying compositions at 220 °C. Obviously, Han plots for neat PMMA and PVDF exhibit quite small spreads, and plots for all of the blends lay between those of components, showing a composition independent correlation; therefore, it indicates a quite good miscibility between PMMA and PVDF from the rheological aspect.

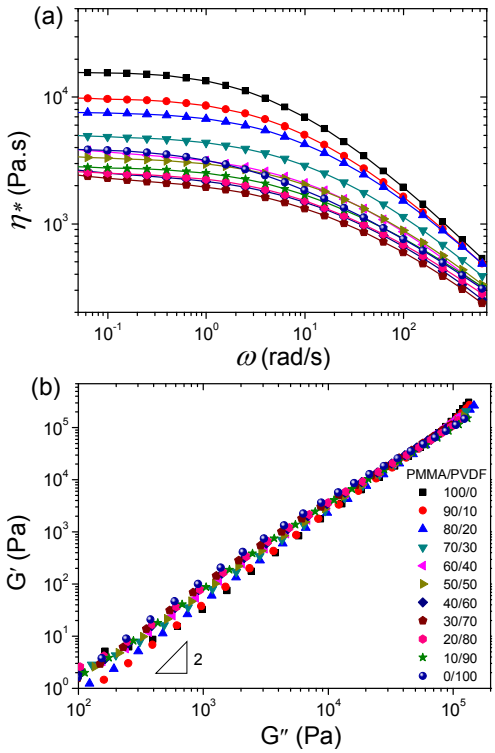

Fig. 1 (a) Complex viscosity versus frequency and (b) Han plots of PVDF/PMMA blends with varying compositions at 220 °C.

Representative curves of time-temperature superposition reduced at a T_{ref} of 220 °C for blends are shown in Fig. 2a-e. At first glance, one can roughly tell that the TTS principle holds well for the blends over all the compositions, with only a subtle discrepancy at the terminal zone. Moreover, a typical terminal behaviour at lower frequencies is observed, *i.e.* $G' \propto \omega^2$ and $G'' \propto \omega$, which is characteristic of a homogeneous blend structure. However, the scenario for TTS emerges a slight difference when one takes careful inspection combining with the curve of phase angle (δ) which is believed to be more sensitive to the failure of TTS principle (Fig. 2).[38] One can observe in Fig. 2 that TTS principle fails for blends with intermediate compositions ($40\% \leq \phi_{PVDF} < 80\%$), especially for those with ϕ_{PVDF} = 60~70%, where the curves of $tan\delta$ are poorly superimposed over the whole terminal zone. In contrast, the TTS failure tends to alleviate in the case of both PMMA-rich blends ($\phi_{PVDF} < 40\%$) (Fig. 2a and 2b) and PVDF-rich blends ($\phi_{PVDF} \geq 80\%$) (Fig. 2e). It should be also pointed out that the data scattering at the lower frequency (below 0.03 rad/s), partly caused by the thermal degradation of PMMA during the longer holding time with higher temperature up to 240 °C , may confuse the judgment on TTS. Fortunately, this effect can be neglected since blends with higher PVDF fractions (*e.g.* 30/70 blend) expected to be more thermally stabile still shows the TTS failure even in the frequency region up to the crossover frequency (ω_c) (Fig.2d). Therefore, this failure of TTS is indicative of differences in the temperature dependence of structural relaxations in blends, *i.e.* dynamic heterogeneity. Meanwhile, temperature dependence of shift factors remain some discrepancies at low temperatures compared to the linearity at high temperatures, implying the less cooperative structural relaxations at low melt temperatures (Fig. 2f). Besides, van Gurp-Palmen (vGP) curves[39] of phase angle (δ) versus complex modulus (G^*) for blends give the same conclusion about the TTS failure (see Appendix A for details). Overall, the degree of thermorheological complexity for blends is composition-dependent: both PMMA- and PVDF-rich blends show a slight thermorheological complexity, whereas blends with intermediate compositions exhibit a moderate one. Compared with PMMA/PEO blends (similar ΔT_g to PMMA/PVDF) where TTS fails severely,[16] PMMA/PVDF blends exhibit the weak thermorheological complexity, likely due to the stronger interactions than the former.

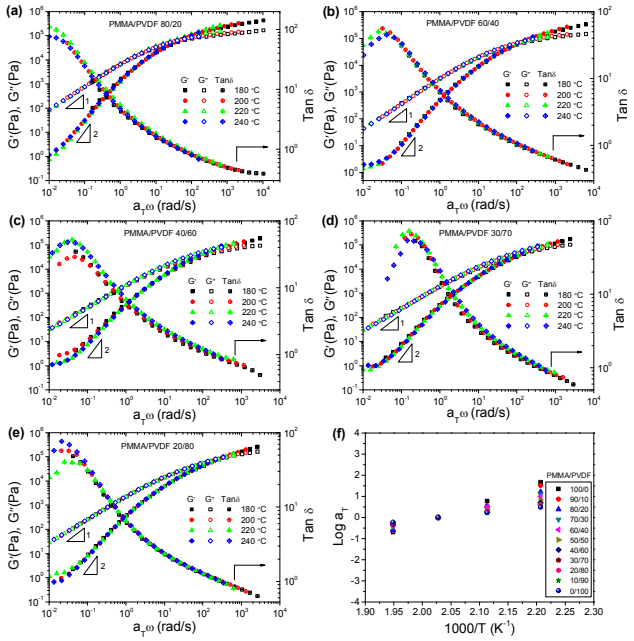

Fig. 2 Time-temperature superposition curves of PMMA/PVDF blends shifted to a reference temperature of 220 °C. (a) PMMA/PVDF (80/20); (b) PMMA/PVDF (60/40); (c) PMMA/PVDF (40/60); (d) PMMA/PVDF (30/70); (e) PMMA/PVDF (20/80); (f) shift factors obtained for the PVDF/PMMA blends with varying compositions using a reference temperature of 220 °C.

Fig. 3a depicts zero-shear viscosity (η_0) estimated by Carreau-Yasuda model[40] for the blends with various compositions. Meanwhile, predicted values of η_0 by two theoretical mixing rules, including the logarithmic additivity rule[41] and logarithmic reciprocal rule,[42] are also given. It is clear that negative deviations for η_0 versus ϕ with respect to mixing rules can be observed, exhibiting a concave up behaviour. More interestingly, instead of monotonic decrease with the inclusion of PVDF, the viscosities of blends with intermediate compositions are lower than those of the components and even emerge a minimum at ϕ_{PVDF} = 60~70%. Besides, weighted relaxation spectrum $\lambda H(\lambda)$ reflecting the time

distribution of chain relaxations was also extracted by the following equation:[43, 44]

$$G^*(\omega) = \int_{-\infty}^{\infty} \frac{H(\lambda) i\omega\lambda}{\lambda(1+i\omega\lambda)} d\lambda \quad (1)$$

where λ is the relaxation time. Fig. 3b illustrates the $\lambda H(\lambda)$ spectra for neat polymers and their blends at 220 °C. Similar to the trend of η_0, the average relaxation times the blends especially at intermediate compositions are shorter than those of the components and also exhibits a minimum for bends with ϕ_{PVDF} = 60~70%, displaying a speed-up in relaxations. Generally, molecular entanglements dictate the viscoelastic properties. It is ever reported that PMMA/PVDF blends can have reduced molecular entanglements in comparison with their components.[45, 46] The observed curve up behaviour and a local minimum in viscosity, as well as the speed-up relaxations for blends with intermediate compositions are assumed to be related with the reduced molecular entanglements, which will be discussed in the next section.

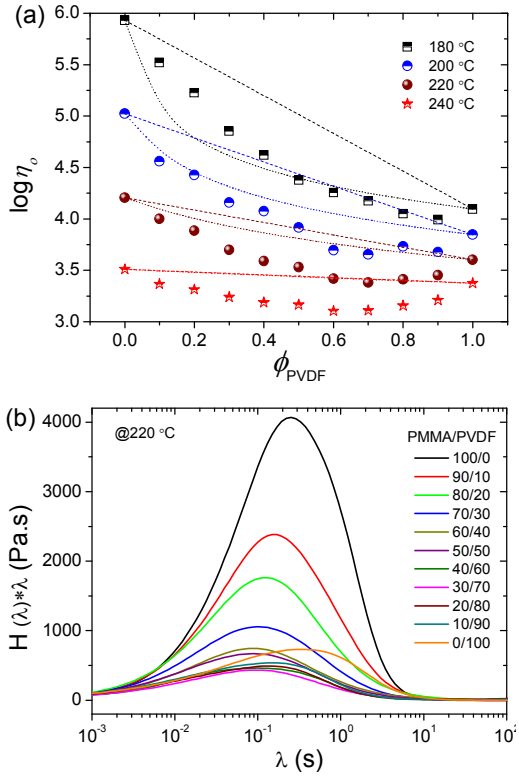

Fig. 3 (a) Plots of zero-shear viscosity versus compositions of PMMA/PVDF blends at temperature range from range from 180 °C to 240 °C (the scatters are the experimental, the dashed and dotted lines are respectively predicted by logarithmic additivity rule and reciprocal mixing rule); (b) weighted relaxation spectra of PMMA/PVDF blends over a wide composition at 220 °C.

3.2 Chain entanglements

The entanglement state of both the similar chains (*i.e.* intrachains) and dissimilar chains (*i.e.* interchains) in PMMA/PVDF blends can be deduced in terms of entanglement molecular weight (M_e) within each component and that (M_{e12}) between two components (see Appendix B for details).[30, 47] For clarity, the parameters on chain entanglements for PMMA/PVDF blends measured at 220 °C are representatively listed in Table 2 and relevant calculations are described in Appendix B. The plateau modulus (G_N^0) for PVDF (*i.e.* 6.23×10^5 Pa) and its entanglement molecular weight (*i.e.* 9.58 kg/mol) at 220 °C agree well with the previously reported values.[48] A slightly higher G_N^0 for PMMA and therefore a little lower M_e compared with the literature data[48] can be due to the semi-quantitive character of the calculation method based on crossover modulus. It can be clearly observed that $M_{e12} > M_e$ ever reported by Wu,[30] which indicates that dissimilar chains are less likely to entangle with each other than the similar chains in PMMA/PVDF blends, is also captured in the present study. The difference from findings of Wu lies in that this kind of entanglement only tends to be pronounced for blends with intermediate compositions (40% ≤ ϕ_{PVDF} < 80%) in our study, whereas it exists over the whole compositions in the case of Wu. The slight deviation of blend with ϕ_{PVDF} = 50% is not clear for the moment and is still being investigated in a future article. As for PMMA-rich blends (ϕ_{PVDF} <40%) and PVDF-rich blends (ϕ_{PVDF} ≥ 80%), however, an opposite scenario, *i.e.* $M_e > M_{e12}$ which implies dissimilar chains can entangle with each other more than similar ones, can be found. Apparently, chain entanglement state in PMMA/PVDF blends also appears the composition dependence. In particular, blends with intermediate compositions have the higher M_e and M_{e12} and the maximum ones for ϕ_{PVDF}=80%, clearly suggesting the reduced molecular entanglement; this is coincided with proceeding assumption, explaining the observed curve up behaviour and a local minimum in viscosity, and speed-up relaxations.

The composition dependence of chain entanglements as observed can be rationalized by invoking the intermolecular interactions. According to the FTIR spectra, intermolecular interactions in the studied blends are strongly dependent on the compositions, where PVDF-rich blends demonstrate the stronger interactions while blends with intermediate compositions display the medium ones (see Fig. S1 in Electronic Supplementary Information). This agrees well with results of Wendorff[6] that this pair of blends shows very large negative value of interaction parameter (χ) with strong composition dependence, where χ is continuously decreased with increasing the content of PVDF but further reduced more steeply for PVDF-rich blends (χ decreases from -0.02 to -0.7). It is also worth mentioning that the value of χ was measured by Wendorff in the melt (i.e. 187 °C),[6] and our group recently obtained a relation χ=0.2207-137.52/T(K) by rheological modelling for the melt mutual-diffusion in PMMA/PVDF bilayers;[7] hence, χ is expected to be negative and interactions persist in the melt temperature ranges under the present study. Therefore, it is envisaged that for PVDF-rich blends dissimilar chains entangle with each other more than the similar chains in the presence of the stronger interactions. Besides, PVDF chains were re-

ported to possess the strong tendency to self-associate rather than inter-associate with PMMA chains.[10, 13] There even exists a nearly pure PVDF interphase which is not penetrated by PMMA in the crystalline blends (*i.e.* $\phi_{PVDF} \geq 40\%$) despite their favourable interactions.[32] Logically, for blends with intermediate compositions having the moderate interactions compared to PVDF-rich blends, the self-association or intrachain entanglements of PVDF chains occurs preferentially and PVDF chains thus have less chance to entangle with PMMA chains.

Table 2 Crossover modulus, plateau modulus, and entanglement molecular weight of PMMA/PVDF blends at 220 °C

PMMA/PVDF (v/v)	G_c ($\times 10^4$ Pa)	G_N^0 ($\times 10^5$ Pa)	M_e (kg/mol)	M_{e12} (kg/mol)
100/0	7.35	4.81	9.22	—
90/10	7.58	5.28	8.72	6.99
80/20	8.52	6.16	7.74	5.82
70/30	7.78	5.74	8.59	7.67
60/40	6.86	5.10	9.98	10.42
50/50	8.26	6.14	8.54	7.61
40/60	7.33	5.41	9.97	10.30
30/70	7.24	5.28	10.49	12.04
20/80	8.54	6.13	9.28	8.47
10/90	10.44	7.33	7.95	4.14
0/100	9.10	6.24	9.57	—

Additionally, one might be further surprised by the case of PMMA-rich blends (ϕ_{PVDF} <40%) where dissimilar chains entangle with each other more than the similar ones, analogous to the case of PVDF-rich blends ($\phi_{PVDF} \geq 80\%$) but the interactions are weaker compared with the latter. It is understandable that rigid PMMA chains (high-T_g) dominate in PMMA-rich blends. One plausible explanation for the entanglement window herein could be ascribed to the large-scale restricted entanglement spacing and/or confined chain surroundings of PVDF by PMMA. In that way, PVDF chains are less likely to self-associate/entangle internally but relax cooperatively with PMMA chains. Besides, it is widely agreed that for PMMA-rich blends, no crystallization takes place either upon slow cooling from the melt or annealing at a temperature above T_g. This suggests that PVDF chains are unable to self-associate to form nucleation in PMMA-rich blends, which further demonstrates that PVDF chains are less likely to entangle themselves but with PMMA chains therein. Moreover, Bose and coworkers[49] recently reported the self-concentration (ϕ_s) of PMMA as 0.05 in PMMA/PVDF (90/10) (w/w) blend (PMMA-rich) under the " self-concentration" model of Lodge-McLeish (LM),[24] which is far below the theoretical value, *i.e.* ϕ_s =0.31.[7] It might also imply that PMMA chains would rather entangle with PVDF chains than self-concentrate in PMMA-rich blends.

As observed, chain entanglement state of PMMA/PVDF blends exhibits the composition dependence similar to that of thermorheological complexity. It is proposed that the scenario of thermorheological complexity for PMMA/PVDF blends is governed by the molecular entanglements. In both PMMA- and PVDF-rich blends, interchains among homopolymers tend to entangle much more than intrachains and thus relax cooperatively, leading to the slight thermorheological complexity; for blends with intermediate compositions, on the contrary, intrachain entanglements prevail and thus dissimilar chains relax less cooperatively, resulting in the medium thermorheological complexity. Other factors including heterogeities can also contribute to the thermorheological complexity, which will be resolved in the following section.

3.3 Dielectric relaxation spectroscopy: local heterogeneity in the melt

Dielectric relaxation spectroscopy (DRS) was employed to further obtain crucial insights into the molecular dynamics in the melt-state PMMA/PVDF blends. Fig. 4 presents the frequency dependence of dielectric loss modulus spectra (M'') for neat polymers and blends at temperatures from 180 to 240 °C (see relevant loss permittivity spectra ε'' in Fig. S2 in Electronic Supplementary Information). Electric modulus formalism is advantageous over others as it suppresses effects of electrode polarization at the lower frequency.[50] To analyse quantitatively the relaxation behaviors, the experimental plots of M'' versus frequency were further fitted by the Havriliak–Negami (HN) equation according to the following form:[50]

$$M' = M_\infty M_0 \frac{\left[M_0 A^\beta + (M_\infty - M_0)\cos\beta\varphi\right]A^\beta}{M_0^2 A^{2\beta} + 2A^\beta (M_\infty - M_0) M_0 \cos\beta\varphi + (M_\infty - M_0)^2} \quad (2)$$

$$M'' = M_\infty M_0 \frac{\left[(M_\infty - M_0)\sin\beta\varphi\right]A^\beta}{M_0^2 A^{2\beta} + 2A^\beta (M_\infty - M_0) M_0 \cos\beta\varphi + (M_\infty - M_0)^2} \quad (3)$$

$$A = \left[1 + 2(\omega\tau_{HN})^\alpha \sin\frac{(1-\alpha)\pi}{2} + (\omega\tau_{HN})^{2\alpha}\right]^{1/2} \quad (4)$$

$$\varphi = arctg\left[\frac{(\omega\tau_{HN})^\alpha \cos\frac{(1-\alpha)\pi}{2}}{1 + (\omega\tau_{HN})^\alpha \sin\frac{(1-\alpha)\pi}{2}}\right] \quad (5)$$

where ε' and ε'' are storage and loss permittivity, M′ and M″ are dielectric storage and loss modulus, M_∞ and M_0 are the high and low frequency limits of M', respectively, $M_\infty = 1/\varepsilon_\infty$ and $M_0 = 1/\varepsilon_0$; ω is the angular frequency ($\omega = 2\pi f$) and α and β shape parameters ($0 < \alpha, \beta \leq 1$). The corresponding fitted M'' plots are shown by solid curves in Fig. 4. It is known that PVDF and PMMA are respectively identified as dielectric type-B and type-C polymer,[51] thus the normal mode relaxation related to the end-to-end vector of whole chains is dielectrically invisible in the DRS spectra. As for neat PMMA (Fig. 4a), the dielectric relaxation has been observed as two relaxations, where one relaxation peak (above 10 kHz) corresponds to the merged $\alpha\beta$ relaxation of α-relaxation (segmental motions) and β-relaxation (local motions of side group),[32]and the other represents the conductivity relaxation with characteristic relaxation time defined by $2\pi f_{max}\tau = 1$. Conductivity relaxation peak symbolizes the transition from long range to short range mobility of charge carriers (catalyst, impurities, etc.) along conductivity paths. By contrast, segmental relaxations of PVDF are not captured in the measured temperature and frequency ranges. The conductivity relaxation of PVDF emerges at higher frequen-

cies (10^4 –10^5 Hz) (Fig. 4b), suggesting the higher mobility of charge carriers in PVDF.

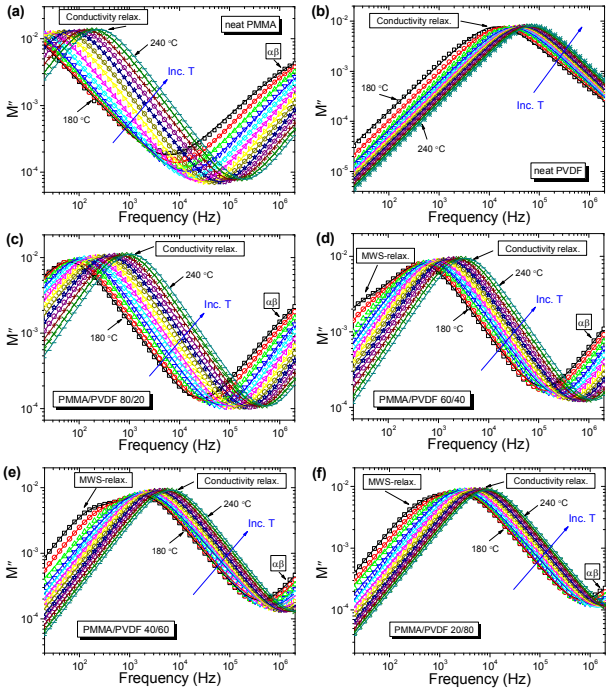

Fig. 4 Dielectric loss modulus *M*″ as a function of frequency with temperature ranging from 180 °C to 240 °C (5 °C increment) for (a) neat PMMA; (b) neat PVDF; (c) PMMA/PVDF (80/20); (d) PMMA/PVDF (60/40); (e) PMMA/PVDF (40/60); (f) PMMA/PVDF (20/80). The solid curves are fitted lines by Havriliak–Negami equation.

As for blends, one can view that the characteristic relaxation frequency (f_{max}) of conductivity relaxation locates between that of neat PMMA and PVDF, and shifts to higher frequencies with increasing temperature and/or PVDF content (Fig. 4c-f). $\alpha\beta$ relaxation shifts to higher frequency accompanied by the declined intensity with increasing PVDF content. Interestingly, for blends ($\phi_{PVDF} \geq 40\%$) a shoulder-like relaxation peak emerges at frequency region below f_{max} particularly at the lower melt temperatures. This shoulder moves to higher frequencies, comes closer to the conductivity relaxation peak with increasing temperature, and are hardly discernible at the higher temperatures (above 220 °C). As mentioned above, normal mode relaxation is dielectrically inert for both PMMA and PVDF, and electrode polarization is greatly suppressed with the electric modulus; hence, the emerging relaxation observed at lower frequency is ascribed to the relaxation of charge carriers at interfaces within the bulk of the sample, *i.e.* interfacial *Maxwell-Wagner-Sillars* (MWS) polarization.[51] It is worthwhile to note that MWS relaxation observed in blends under investigation displays a composition dependence. To clearly illustrate the trends, the normalized *M*″ curves of blends ($\phi_{PVDF} \geq 20\%$) for the conductivity relaxation, *i.e.* M''/M''_{max} versus f/f_{max}, are plotted in Fig. 5. Notably, MWS relaxation peak becomes most pronounced for blends with ϕ_{PVDF} increased up to 60%, but further declines for PVDF-rich blends ($\phi_{PVDF} \geq 80\%$) (Fig. 5a). At higher temperatures (*e.g.* 220 °C), MWS relaxation tends to be merged with the conductivity relaxation (Fig. 5b). With relaxations both in the blend bulk (*i.e.* conductivity relaxation) and at the interface (*i.e.* MWS relaxation), charge carriers shows a bimodal relaxation behaviour, especially in the blends ($40\% \leq \phi_{PVDF} < 80\%$). Further analysis on the dielectric relaxation behaviors by Cole-Cole plot (*M*″~*M*′) and alternating current conductivity (σ_{AC}) also suggests the bimodal relaxation of charge carriers in these blends (Fig. S3 and S4 in Electronic Supplementary Information).

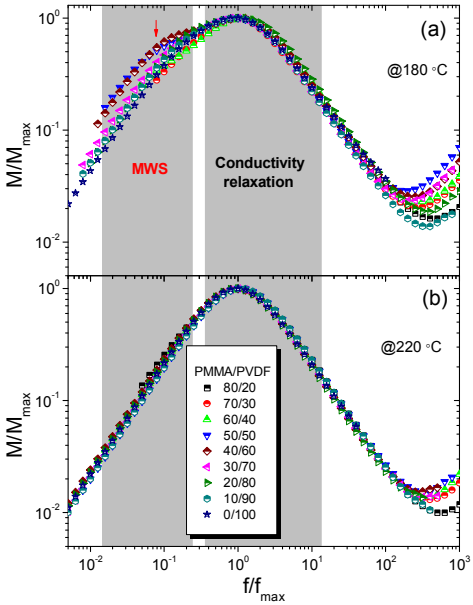

Fig. 5 Normalized frequency dependence of *M*″ for the conductivity relaxation of PMMA/PVDF blends with various compositions at 180 °C (a) and 220 °C (b)

Charge carrier transport is governed by the motion of the polymer chains at temperatures higher than T_g.[52] The dynamics of charge carriers can thus reflect the structural relaxations of blends. Fig. 6a represents the plots of f_{max} versus the reciprocal temperature for the conductivity relaxation. The temperature dependence of the conductivity relaxation can be well described by the Arrhenius equation:

$$f_{max} = A \exp\left(-\frac{E_a}{RT}\right) \quad (6)$$

where A is the pre-exponential factor, E_a is the activation energy, R is the gas constant, respectively. E_a was determined by performing the least square fit to the plots and has been shown in Fig. 6b. Schematical deconvolution for the relaxations by HN equation is shown by Fig. 6d. One can observe that the activation energy for the conductivity relaxation is continuously reduced with the increase of PVDF. For comparison, the activation energy of the viscous flow obtained from the rheological test is also presented. In principle, E_a from rheology reflects the activation barrier of

chain relaxations, while E_a from DRS shows that of charge carrier transport. Interestingly, the values of E_a obtained from DRS are in harmony with these estimated from rheology despite some small disparities in PMMA-rich blends, confirming that charge carrier transport is governed by the motion of chains in the blends under investigation. Increasing the content of PVDF (low-T_g component) leads to an increase in the mobility of chains in blends and accelerates charge carrier transport. The slight deviation E_a by DRS from that by rheology for PMMA-rich blends is presumably due to uneven distribution of charge carriers around the PMMA backbone and side-groups, where the charge carriers around the side-groups moves with less activation barriers. The plots of f_{max} as a function of composition for both conductivity relaxation and MWS at 180 °C are shown in Fig. 6c. It is evident that relaxation times of two processes nearly show similar composition dependence and both decline with increasing PMMA content, indicating that the addition of PMMA (high-T_g component) imposes constraint on the structural relaxations at both the interfaces and the blend bulk. Besides, the slower MWS relaxation than conductivity relaxation is attributed to the hindered motions of charge carriers blocked at the interfaces.

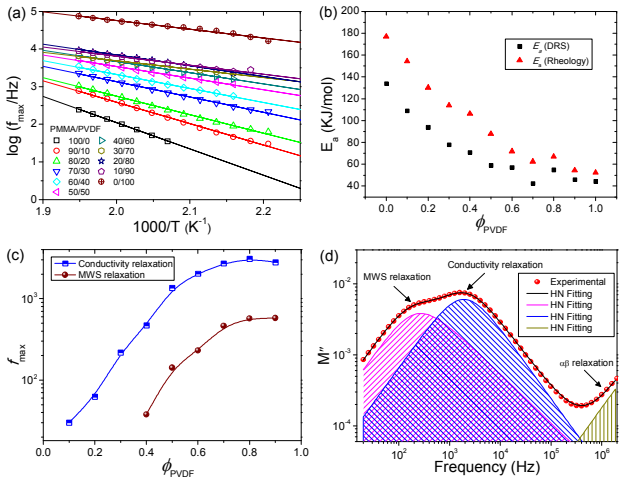

Fig. 6 (a) Activation plots of the conductivity relaxation process for PMMA/PVDF blends with various compositions; (b) plots of activation energy estimated from rheological test and DRS test for PMMA/PVDF blends; (c) plots of the characteristic relaxation frequency for conductivity relaxation and MWS relaxation process of blends at 180 °C; (d) schematic deconvolution for the curves of loss modulus versus frequency.

The presence of bimodal relaxation of charge carriers associated with MWS relaxation in the melt-state blends is a clear indication of the coexistence of distinct environments. The origin for this type of heterogeneity can be addressed by the multiphase morphology of PMMA/PVDF blends in the solid and its evolution in the melt. Blends with $\phi_{PVDF} \geq$ 40% are crystallizable upon cooling from the melt and phase separation occurs in sequence (DSC results in Fig. S5 and Table S1 of Electronic Supplementary Information). The resulting morphology of crystalline blends consists of a crystalline PVDF phase, an amorphous phase, as well as a crystal-amorphous interphase.[32, 33] The amorphous phase is the miscible amorphous PMMA/PVDF blends, while the interphase is solely comprised of PVDF from which PMMA has been excluded during crystallization (Fig. 7a).[32, 34] Upon melting, all chains of both components relax, diffuse and gradually lose their original conformation. From a microscopic viewpoint, in addition to constraining tubes constructed by neighbouring chains of the same polymer, the interactions between a wriggling chain and its neighbouring chains of the other polymer also contribute to the establishment of new entanglements, as a result of mutual diffusion of PMMA and PVDF chains. Particularly, in the original interphase and crystal regions, *i.e.* PMMA-free regions, PVDF chains gradually entangle with the diffused PMMA chains from the original amorphous miscible phase. Unfortunately, PVDF chains usually tend to be self-associated rather than entangled with PMMA chains, [27, 30] which is especially true for blends at the intermediate compositions as discussed earlier. Therefore, PVDF chains are unable to largely entangle with PMMA chains therein. Those regions, which are originally devoid of PMMA, are unlikely to achieve completely identical to the remaining regions (original amorphous phase), but act as transition region between the latter in the melt. This transition region can be regarded as a new interphase, *termed as* "Interphase II", as schematically shown in Fig. 7a. It is logical that the blends contain two distinct local regions: Region A (derived from the amorphous miscible phase) and Region B (Interphase II) (Fig. 7a); the structural asymmetries between them determine the degree of local heterogeneity. The entanglement state of the interphase in the melt should also depend on its inner composition. Understandably, the local concentration of PMMA in the Region A is reduced due to the removal of PMMA chains by its diffusion. At higher blend concentration of PVDF, *i.e.* PVDF-rich blends, it is expected that those PMMA-free regions easily admit the diffused PMMA chains because of the favourable interchain entanglements (stronger interactions for PVDF-rich blends). Consequently, both regions can have the comparable local compositions and thus equivalent entanglement state, alleviating the degree of heterogeneity. This can account for the observed reduced intensity of MWS relaxation for blends with $\phi_{PVDF} \geq$ 80% (Fig. 5a). By contrast, the degree of heterogeneity in the blends (40% $\leq \phi_{PVDF} <$ 60%) in the melt declines with decreasing PVDF content. It is caused by the thinner crystal and interphase at solid state, into which PMMA chains can penetrate more effectively on melting. Region B thus has less difference from Region A, and the entire blend becomes less heterogeneous with decreasing PVDF. Especially, blend ($\phi_{PVDF} \approx$ 60%) is demonstrated to have the largest degree of local heterogeneity, suggesting the highest asymmetry in entanglement state between Region A and B. Herein, Region B should possess the much lower entanglement density than Region A. Overall, it is assumed that the interphase in the melt has the weaker entanglements than the remaining regions (Region A). The deviation in entanglement density of interphase from that of Region A leads to the coexistence

of two distinct environments. Besides, one can also expect that this kind of interphase survives upon statically annealing at higher temperatures in view of its inner unfavourable interchain entanglements, despite the diminishing intensity in MWS relaxation with increasing temperature.

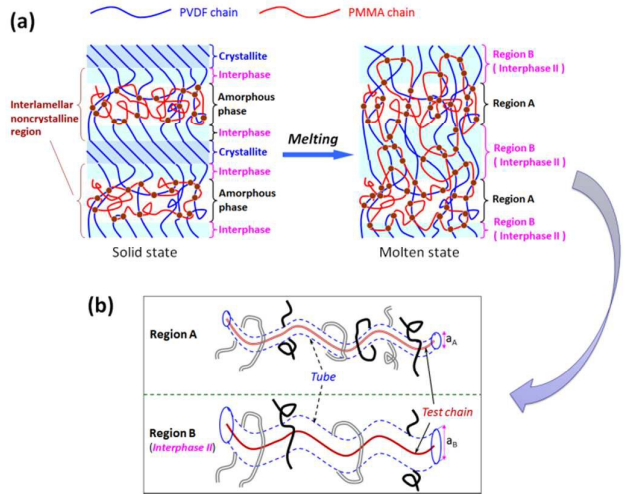

Fig. 7 (a) Schematic of morphology evolution for crystalline PMMA/PVDF blends from solid state to molten state. (b) Schematic of a hypothetical tube concept.

Bearing in mind the presence of interphase in the melt, one can further elucidate its effects on the viscoelastic behaviours and overall thermorheological complexity of blends. As described above, in Region B (interphase II), the unfavourable interchain entanglement probability between PMMA and PVDF chains results in a weak entanglement fraction as compared to Region A. Besides, our recent study also revealed that the diffuse interphase in the PMMA/PVDF bilayer has the dilated tube (larger tube diameter) due to weak entanglements.[53] This conclusion seems to hold true for the interphase presented here, since both of them are triggered by interdiffusion among PMMA and PVDF chains. It is therefore expected that dilated tube prevails in the Region B assuming its same physics of weak topological constraint with the diffuse interphase. Presumably, the tube diameter of Region B is larger than Region A ($a_B > a_A$), as schematically shown by a hypothetical tube concept (Fig. 7b). In the melt, the structural relaxations with released constraint in interphase (Region B), which can be treated as effective solvent for the remaining regions, facilitates the overall relaxations in the blends. As observed, blends (40% $\leq \phi_{PVDF} <$ 80%) of which the interphase is more pronounced in the melt exhibit the reduced viscosities and speed-up relaxations, especially for blend ($\phi_{PVDF} \approx$ 60%) (Fig. 3). The presence of interphase in the melt, coupled with the unfavourable interchain entanglement, is thus responsible for the lower viscosity and speed-up relaxations in those blends. It is also concluded that the distinct relaxation of interphase contributes to the degree of thermorheological complexity of blends, since blends (40% $\leq \phi_{PVDF} <$ 80%) with more obvious interphase display the moderate thermorheological complexity and the particular blend ($\phi_{PVDF} \approx$ 60%) shows the greatest thermorheological complexity (Fig. 2c). Especially, the more notable relaxation of interphase, coupled with less cooperative motions of chains, results in the deviation of shift factor *versus* temperature from linearity at low melt temperatures (Fig. 2f).

3.4 Effects of dynamic heterogeneity on the glass transition temperatures and dynamic mechanical properties

The glass transition temperatures of PMMA/PVDF blends with various compositions were determined both by DSC and DMA. Values of T_g taken from the inflection point of the glass transition with DSC are shown by the round scatters in Fig. 8. The temperature, at which a sharp decrease in storage modulus (E'), loss modulus (E'') and damping factor ($tan\delta$) exhibit a peak in DMA thermograms, also corresponds to the glass transition temperature (Fig. 9). Values of T_g discerned from peak temperature of E'' are also plotted by the triangle scatters in Fig. 8. It can be observed that T_g measured by DSC agrees quantitatively with that by DMA, despite the slightly higher T_g by DMA (40% $\leq \phi_{PVDF} \leq$ 60%) caused by crystallization in as-prepared DMA samples. It is apparent that the bends at low concentration of PVDF (ϕ_{PVDF} <40%) shows a single but broader T_g. However, two T_gs can be clearly observed for blends with higher concentration of PVDF ($\phi_{PVDF} \geq$60%). The existence of two T_gs is derived from the multiphase morphology of crystalline PMMA/PVDF blends. The T_g at higher temperature ($T_{g,1}$) corresponds to the T_g of the amorphous miscible phase.[30] As observed, $T_{g,1}$ shifts from the T_g of PMMA (*i.e.* 112 °C) to the lower temperature as PVDF content increases. The abrupt increase in $T_{g,1}$ is observed for blends ($\phi_{PVDF} >$ 40%) due to the local trapping of PMMA into the amorphous phase during crystallization where local concentration of PMMA is higher than that of the bulk.[8] Besides, one might assume that the other T_g at lower temperature ($T_{g,2}$) is attributed to segmental relaxation of the PVDF in the amorphous phase. This assumption, however, contradicts the observed moderate shift in $T_{g,2}$ to higher temperatures with increasing PVDF (the insets of Fig. 9). This shift was also observed by Paul *et al.*[5] Therefore, in this study it is proposed that the origin of $T_{g,2}$ could be related with crystal-amorphous interphase (only PVDF segments) in the blends. On increasing PVDF in blends, the crystalline phase will be more perfect and thicker, evidenced by the increase in melting temperature (T_m) (Fig. S5 and Table S1 in the Electronic Supplementary Information). With larger confinement to interphase imposed by the thicker PVDF crystals, segments in the interphase are thus observed to relax at the higher temperatures (*i.e.* higher $T_{g,2}$). $T_{g,2}$ was not captured for blends (40% $\leq \phi_{PVDF} \leq$ 60%) due to the resolution limitation of DSC and DMA employed in this study.

To study the effective glass transition ($T_{g,eff}$), the "self-concentration" model of Lodge-McLeish (LM) [24] is employed with considering the dynamic heterogeneity. This model associates the average local concentration (ϕ_{eff}) for each component with a local glass transition temperature:

$$\phi_{eff,A} = \phi_{s,A} + (1-\phi_{s,A})\phi_A \quad (7)$$

where $\phi_{eff,A}$ is the effective concentration of a given component A (the same for component B), $\phi_{s,A}$ is its self-concentration, and ϕ_A is the bulk composition of the blend, respectively. According to LM model, each component in the blend experiences a distinct effective glass transition temperature that depends on ϕ_{eff}. $T_{g,eff}$ for component A can be determined from ϕ_{eff} via the modified Fox equation:

$$\frac{1}{T_{g,eff,A}} = \frac{\phi_{eff,A}}{T_{g,A}} + \frac{1-\phi_{eff,A}}{T_{g,B}} \quad (8)$$

For the calculation the $T_{g,eff}$, self-concentration (ϕ_s) of PMMA and PVDF are respectively take as 0.31 and 0.32, for which the calculation details were given in our previous study.[7] The calculated values of $T_{g,eff}$ for PMMA and PVDF are plotted with dashed lines in Fig. 8, together with the theoretical T_g via Fox equation with the solid line. Clearly, Fox equation fails to describe the experimental T_g. Instead, the $T_{g,eff}$ of PMMA predicted by LM model is very close to the experimental for the amorphous blends ($\phi_{PVDF} < 40\%$). Whereas, crystallization denies the LM model for the crystalline blends where $T_{g,eff}$ of PMMA is illogically lower than $T_{g,1}$. Fortunately, the equivalent local composition of the amorphous miscible phase in crystalline blends can be determined by the approximation from the composition in the amorphous blends ($\phi_{PVDF} < 40\%$), since $T_{g,1}$ shows the similar composition dependence as that of the latter. Furthermore, the $T_{g,eff}$ for crystalline blends is further evaluated with LM model by substituting the equivalent local composition of the miscible phase for the bulk composition, and the values ($T_{g,eff}'$) are plotted with dotted lines in Fig. 8. The agreement of $T_{g,eff}'$ for PMMA with the experimental $T_{g,1}$ is now acceptable for the crystalline blends with the approximation for local composition of the miscible phase. The abrupt increase in $T_{g,eff}'$ of PVDF is due to higher local concentration of PMMA than the bulk, which causes lager confinement to PVDF segments as the case of PMMA-rich blends.

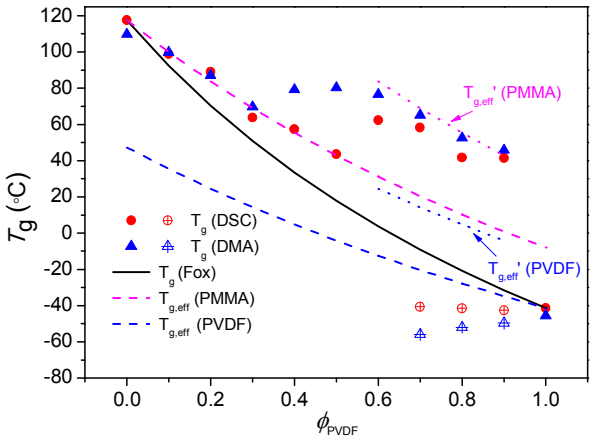

Fig. 8 Glass transition temperature of PMMA/PVDF blends as determined by DSC and DMA (scatters), and predicted by theories (lines).

In accordance with LM model, as seen in Fig. 8, the high-T_g component (*i.e.* PMMA) in the blends over the whole compositions shows $T_{g,eff}$ closer to the blend average, whereas $T_{g,eff}$ of low-T_g component (PVDF) is nearer to that of neat PVDF. Considering the better description of experimental T_gs with LM model (Fig. 8), one can view that crystalline blends, especially with intermediate compopitions ($40\% \le \phi_{PVDF} \le 60\%$), show three distinct values of $T_{g,eff}$, of which the largest one ($T_{g,eff}'$) is related to PMMA segments in miscible phase, the medium one to the PVDF segments in miscible phase, and the smallest one ($T_{g,2}$) to PVDF segments within the crystal-amorphous interphase; hence, three distinct segment dynamics are expected therein. Besides, differences between $T_{g,2}$ and $T_{g,eff}$ of PVDF or PMMA are clearly larger for blends with intermediate compositions, likely indicating the more prominent heterogeneity in segment dynamics. Particularly, one can also expect the largest dynamic heterogeneity in blend with $\phi_{PVDF} \approx 60\%$, for which there emerge the biggest differences among the values of $T_{g,eff}$. Therefore, the presence of crystal-amorphous interphase with distinct relaxation contributes to the dynamic heterogeneity for PMMA/PVDF blends at the solid state. Specifically, three distinct relaxation dynamics of segments are supposed to exist in blends with intermediate compositions, leading to the larger dynamic heterogeneity.

Apart from the glass transition, the dynamic mechanical properties also show a strong dependence of composition (Fig. 9). As observed, the damping factor is clearly larger for PMMA-rich blends (*e.g.* $\phi_{PVDF} = 20\%$) and negligibly decreases with the addition of PVDF (*i.e.* low damping component). It seems that PVDF segments experience large-scale confinement imposed by rigid PMMA segments in PMMA-rich blends, as explained earlier. Notably, the dynamic mechanical behaviours appear alike among PMMA-rich blends manifesting in the analogous shape of curves, which is the same case for PVDF-rich blends. Presumably, they are attributed to the prevailing interchain entanglements and relatively cooperative relaxations of segments. It is also noteworthy that the dynamic mechanical thermograms for blends at intermediate compositions show obvious deviations from those of remaining blends, which is a clear response of distinct segmental dynamics in the presence of crystal-amorphous interphase as discussed above. It is therefore concluded that the dynamic heterogeneity associated with the crystal-amorphous interphase in the PMMA/PVDF blends remarkably affects dynamic mechanical properties. This part presented here is a guideline for the studies regarding the effects of segmental dynamic heterogeneity on the glass transitions and macroscopically dynamic mechanical properties of PMMA/PVDF blends. Nevertheless, more investigations will be carried out to enrich these interpretations on basis of component segment dynamics.

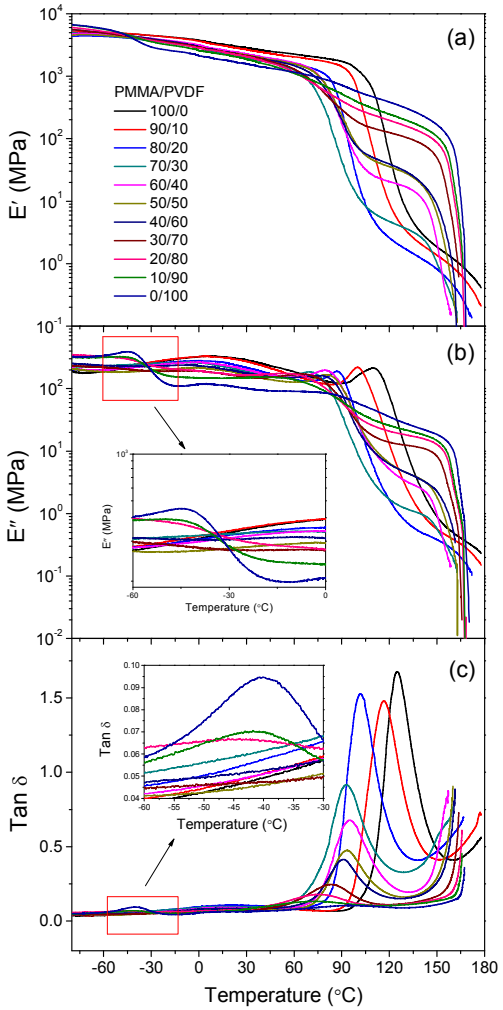

Fig. 9 (a) Storage modulus (E'), (b) loss modulus (E''), and (c) damping factor ($tan\delta$) as a function of temperature obtained by DMA for PMMA/PVDF blends with various compositions.

4. Conclusions

In this work, dynamic heterogeneity in PMMA/PVDF blends was studied with regard to microscopic dynamics and macroscopic properties, and its composition dependence and the role of interphase were elaborated. Firstly, the composition dependence of thermorheological complexity in the melt was clearly mapped. Molecular entanglement state was found to govern the scenario of thermorheological complexity in view of chain entanglements involving intra- and interchain entanglements. Secondly, local heterogeneity was further demonstrated to exist in the melt-state blends with intermediate compositions manifesting in the distinct MWS relaxation, and its origin was depicted to be the interphase. This interphase, coupled with unfavourable interchain entanglements, could account for the reduced viscosity and speed-up relaxations as observed in those blends, favourable for the overall thermorheological complexity. Thirdly, two experimental T_gs of blends were resolved in light of the multiphase morphology of crystalline blends, and further assessed on the basis of the "self-concentration" concept. Three distinct relaxation dynamics of segments were supposed to prevail in the blends with intermediate compositions. The presence of the crystal-amorphous interphase thus contributes to the dynamic heterogeneity in segment relaxations for PMMA/PVDF blends at the solid state. In addition, dynamic mechanical properties of PMMA/PVDF blends were also evaluated. Dynamic heterogeneity associated with the crystal-amorphous interphase in the PMMA/PVDF blends remarkably affects dynamic mechanical properties. Hopefully the results presented here will guide the understanding of the dynamics of this blend pair at molecular scale and the design of tailor-made electrolytes or smart devices (e.g. capacitors) based on them.

Appendix

A. Van Gurp- Palmen (vGP) curves

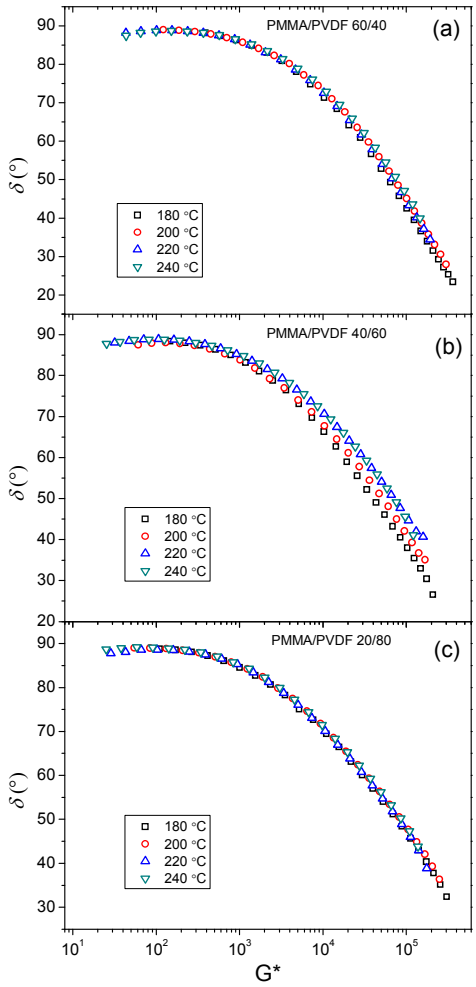

Fig. 10 Representative vGP curves for PMMA/PVDF blends over temperature range from 180 °C to 240 °C. (a) PMMA/PVDF (60/40); (b) PMMA/PVDF (40/60); (c) PMMA/PVDF (20/80).

Phase angle (δ) was plotted against complex modulus (G^*) according to van Gurp and Palmen method.[39] This way of plotting eliminates the effect of shifting along the frequency axis and yields temperature-independent curves when TTS holds. Moreover, the amount of a resulting vertical shift can readily observed with vGP curve, which allows of the complete identification of the thermorheological simplicity or complexity. For the sake of brevity, the vGP curves of PMMA/PVDF (60/40), (40/60) and (20/80) blends are representatively shown in Fig. 10. Identical to the trends in Time-temperature superposition curves (Fig. 2), the failure of TTS displays the composition dependence and is more severe for blends with intermediate compositions, but alleviates for the PMMA- and PVDF-rich blends (Fig. 10).

B. Calculation of entanglement molecular weights

Entanglement molecular weight (M_e), defined as the average molecular weight between adjacent temporary entanglement points, is one of the most fundamental parameters for polymeric material. Generally, M_e is evaluated from the plateau modulus (G_N^0), which can be determined by measuring the storage modulus and the loss modulus in rheological test.[54]

$$G_N^0 = \frac{\rho RT}{M_e} \tag{9}$$

where ρ is the density at the chosen reference temperature T, and R is the gas constant. G_N^0 is usually obtained by the G' at the frequency where $tan\delta$ ($tan\delta = G''/G'$) (or G'') exhibits a minimum in the plateau zone or by the numerical integration over the terminal relaxation peak of $G''(\omega)$.[55] However, both $tan\delta$ and G'' exhibit no minimum, and G'' shows no terminal peak over the test frequency regions for PMMA/PVDF blends. So the above are not applicable for the extraction of G_N^0. Instead, another semi-quantitative method based on the crossover modulus G_c (G_c=G'=G'') proposed by Wu[47] is applied.

$$\log\left(\frac{G_N^0}{G_c}\right) = 0.38 + \frac{2.63\log(M_w/M_n)}{1+2.45\log(M_w/M_n)} \tag{10}$$

The weight average molecular weight (M_w) and number average molecular weight (M_n) for the blends were calculated using

$$M_w = w_1 M_{w1} + w_2 M_{w2}, \quad 1/M_n = w_1/M_{n1} + w_2/M_{n2} \tag{11}$$

in which, w is the weight fraction, and the subscripts 1 and 2 refer to the component 1 and 2, respectively.

For a binary blend consisting of volume fraction ϕ_1 and ϕ_2, there are three possible kinds of entanglement points: 1-1, 2-2, and 1-2, *i.e.* intra- and interchain entanglements. Assuming that the probability of every contact between two chains of species i and j is P_{ij} in a unit volume of the blend, the number of contacts between two similar chains is proportional to ϕ_k^2 (k=i,j), and that between two dissimilar chains is proportional to $2\phi_1\phi_2$. Thus, the total number of entanglement points per unit volume is

$$\rho/M_e = P_{11}\phi_1^2 + P_{22}\phi_2^2 + 2P_{12}\phi_1\phi_2 \tag{12}$$

in which, P_{11}=ρ_1/M_{e1}, P_{22}=ρ_2/M_{e2} and P_{12}=$(\rho_1\rho_2)^{1/2}/M_{e12}$. M_{e1} and M_{e2} are respectively the entanglement molecular weights of component 1 and 2, and M_{e12} is that of a hypothetical pure component of density $(\rho_1\rho_2)^{1/2}$ having the same entanglement probability as between the dissimilar chains in the blends.[30, 47] Taking *Eq.* (9) and (12), the following formula is obtained:

$$G_N^0 = \phi_1^2 G_{N1}^0 + \phi_2^2 G_{N2}^0 + \frac{2\phi_1\phi_2 RT\sqrt{\rho_1\rho_2}}{M_{e12}} \tag{13}$$

Note that the densities of the constituent homopolymers change with temperature, and those of the blends vary accordingly as a function of temperature and composition. Therefore, it is necessary to determine the densities in order to quantify correctly the entanglement state. For PMMA and PVDF, their densities (ρ, in g/cm^3) as a function of temperature (T, in °C) above T_g can be determined according to the *Eq.* (14) and (15), respectively.[56]

$$\rho_{PMMA} = 1.223 - 5.29\times10^{-4}T - 0.507\times10^{-6}T^2 \tag{14}$$

$$\rho_{PVDF} = 1.816 - 26.77\times10^{-4}T + 4.75\times10^{-6}T^2 \tag{15}$$

Meanwhile, the density of the blends can be taken as a function of composition:[30]

$$1/\rho = w_{PMMA}/\rho_{PMMA} + w_{PVDF}/\rho_{PVDF} \tag{16}$$

Acknowledgment

The authors would like to express their appreciation to the reviewers for their constructive and meticulous assessment of this work. They thank ARKEMA for providing the polymers. B. L. also acknowledges the China Scholarship Council for providing the doctoral scholarship.

References

1 I. Nicotera, L. Coppola, C. Oliviero, M. Castriota and E. Cazzanelli, *Solid State Ionics*, 2006, **177**, 581-588.
2 S. J. Kang, Y. J. Park, I. Bae, K. J. Kim, H. C. Kim, S. Bauer, E. L. Thomas and C. Park, *Adv. Funct. Mater.*, 2009, **19**, 2812-2818.
3 H. Zhang, P. Zhang, Z. Li, M. Sun, Y. Wu and H. Wu, *Electrochem. Commun.*, 2007, **9**, 1700-1703.
4 T. Nishi and T. Wang, *Macromolecules*, 1975, **8**, 909-915.
5 D. Paul, J. Altamirano and N. Platzer, *Adv. Chem. Ser.*, 1975, 371-385.
6 J. Wendorff, *J. Polym. Sci., Polym. Lett. Ed.*, 1980, **18**, 439-445.
7 H. Zhang, K. Lamnawar and A. Maazouz, *Macromolecules*, 2013, **46**, 276-299.
8 M. Sharma, G. Madras and S. Bose, *Macromolecules*, 2014, **47**, 1392-1402.
9 G. C. Chung, J. A. Kornfield and S. D. Smith, *Macromolecules*, 1994, **27**, 964-973.

10 A. Alegria, J. Colmenero, K. L. Ngai and C. M. Roland, *Macromolecules*, 1994, **27**, 4486-4492.
11 J. A. Pathak, S. K. Kumar and R. H. Colby, *Macromolecules*, 2004, **37**, 6994-7000.
12 T. Sakaguchi, N. Taniguchi, O. Urakawa and K. Adachi, *Macromolecules*, 2005, **38**, 422-428.
13 J. A. Zawada, G. G. Fuller, R. H. Colby, L. J. Fetters and J. Roovers, *Macromolecules*, 1994, **27**, 6861-6870.
14 H. Watanabe, M. Yamazaki, H. Yoshida, K. Adachi and T. Kotaka, *Macromolecules*, 1991, **24**, 5365-5371.
15 J. H. Lee, L. J. Fetters, L. A. Archer and A. F. Halasa, *Macromolecules*, 2005, **38**, 3917-3932.
16 R. H. Colby, *Polymer*, 1989, **30**, 1275-1278.
17 T. R. Lutz, Y. He, M. D. Ediger, H. Cao, G. Lin and A. A. Jones, *Macromolecules*, 2003, **36**, 1724-1730.
18 T. P. Lodge, E. R. Wood and J. C. Haley, *J. Polym. Sci., Part B: Polym. Phys.*, 2006, **44**, 756-763.
19 J. Colmenero and A. Arbe, *Soft Matter*, 2007, **3**, 1474-1485.
20 H. Watanabe and O. Urakawa, *Korea-Aust. Rheol. J.*, 2009, **21**, 235-244.
21 Y. Takahashi, in *Encyclopedia of Polymeric Nanomaterials*, eds. S. Kobayashi and K. Müllen, Springer, Berlin-Heidelberg, 2015, ch. 69, pp. 642-646.
22 G. Katana, E. W. Fischer, T. Hack, V. Abetz and F. Kremer, *Macromolecules*, 1995, **28**, 2714-2722.
23 S. K. Kumar, R. H. Colby, S. H. Anastasiadis and G. Fytas, *J. Chem. Phys.*, 1996, **105**, 3777-3788.
24 T. P. Lodge and T. C. McLeish, *Macromolecules*, 2000, **33**, 5278-5284.
25 R. Kant, S. K. Kumar and R. H. Colby, *Macromolecules*, 2003, **36**, 10087-10094.
26 H.-H. Yang, C. D. Han and J. K. Kim, *Polymer*, 1994, **35**, 1503-1511.
27 S. S. Es‐Haghi, A. Yousefi and A. Oromiehie, *J. Polym. Sci., Part B: Polym. Phys.*, 2007, **45**, 2860-2870.
28 Z. Yang and C. D. Han, *Macromolecules*, 2008, **41**, 2104-2118.
29 A. N. Gaikwad, A. Choperena, P. C. Painter and T. P. Lodge, *Macromolecules*, 2010, **43**, 4814-4821.
30 S. Wu, *J. Polym. Sci., Part B: Polym. Phys.*, 1987, **25**, 557-566.
31 Y. Zhang, M. Zuo, Y. Song, X. Yan and Q. Zheng, *Compos. Sci. Technol.*, 2015, **106**, 39-46.
32 J. Mijovic, J.-W. Sy and T. Kwei, *Macromolecules*, 1997, **30**, 3042-3050.
33 B. Hahn, J. Wendorff and D. Y. Yoon, *Macromolecules*, 1985, **18**, 718-721.
34 B. Hahn, O. Herrmann-Schönherr and J. Wendorff, *Polymer*, 1987, **28**, 201-208.
35 K. Lamnawar and A. Maazouz, *Rheol. Acta*, 2008, **47**, 383-397.
36 C. D. Han and J. K. Kim, *Macromolecules*, 1989, **22**, 1914-1921.
37 C. D. Han and J. K. Kim, *Macromolecules*, 1989, **22**, 4292-4302.
38 J. A. Pathak, R. H. Colby, S. Y. Kamath, S. K. Kumar and R. Stadler, *Macromolecules*, 1998, **31**, 8988-8997.
39 M. Van Gurp and J. Palmen, *Rheol. Bull.*, 1998, **67**, 5-8.
40 K. Yasuda, R. Armstrong and R. Cohen, *Rheol. Acta*, 1981, **20**, 163-178.
41 L. Utracki and M. Kamal, *Polym. Eng. Sci.*, 1982, **22**, 96.
42 H. Van Oene, *Rheology of polymer blends and dispersions*, Academic Press, San Diego, 1978.
43 D. Mead, *J. Rheol.*, 1994, **38**, 1769-1795.
44 J. Honerkamp and J. Weese, *Rheol. Acta*, 1993, **32**, 65-73.
45 S. Wu, *J. Polym. Sci., Part B: Polym. Phys.*, 1987, **25**, 2511-2529.
46 H. K. Chuang and C. D. Han, *J. Appl. Polym. Sci.*, 1984, **29**, 2205-2229.
47 S. Wu, *J. Polym. Sci., Part B: Polym. Phys.*, 1989, **27**, 723-741.
48 H. Zhang, K. Lamnawar and A. Maazouz, *Rheol. Acta*, 2012, **51**, 691-711.
49 M. Sharma, G. Madras and S. Bose, *Macromolecules*, 2015, **48**, 2740-2750.
50 G. Tsangaris, G. Psarras and N. Kouloumbi, *J. Mater. Sci.*, 1998, **33**, 2027-2037.
51 F. Kremer and A. Schönhals, *Broadband Dielectric Spectroscopy*, Springer, Berlin-Heidelberg, 2003.
52 H. Lu, X. Zhang and H. Zhang, *J. Appl. Phys.*, 2006, **100**, 054104.
53 H. Zhang, K. Lamnawar, A. Maazouz and J. M. Maia, *J. Rheol.*, 2016, **60**, 1-23.
54 J. D. Ferry, *Viscoelastic properties of polymers*, Wiley, New York, 1980.
55 C. Liu, J. He, E. Van Ruymbeke, R. Keunings and C. Bailly, *Polymer*, 2006, **47**, 4461-4479.
56 R. Orwoll, in *Physical Properties of Polymers Handbook*, ed. J. Mark, Springer New York, 2007, ch. 7, pp. 93-101.

Graphical Abstract

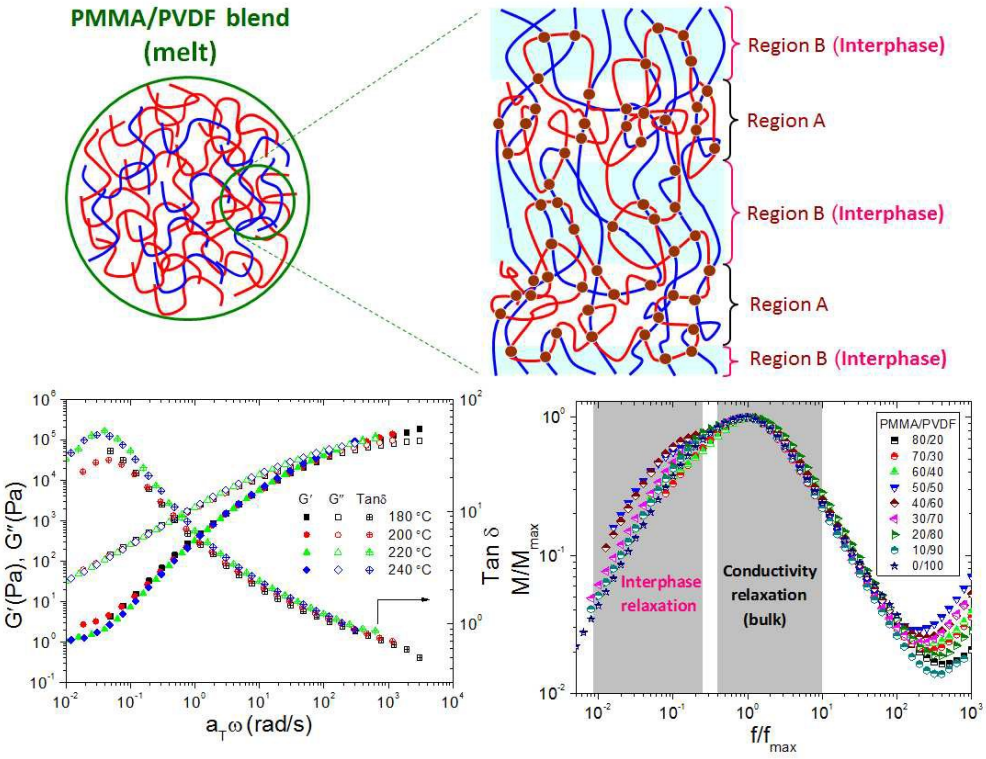

A fundamental study of the dynamic heterogeneity in the PMMA/PVDF blend from the microscopic dynamics to macroscopic properties is presented. The findings can stimulate the understanding this pair of blend at the molecular scale, as well as the design of tailor-made polymer electrolytes and smart devices based on it.